

Supporting Information

All-in-One: Branched Macromolecule-protected Metal Nanocrystals as Integrated Charge Separation/Motion Centers for Enhanced Photocatalytic Selective Organic Transformation

Qiao-Ling Mo, Xin Lin, Zhi-Quan Wei, Xiao-Cheng Dai, Shuo Hou, Tao Li, Fang-Xing Xiao*

College of Materials Science and Engineering, Fuzhou University, New Campus, Minhou, Fujian Province,
350108, China.

E-mail: fx Xiao@fzu.edu.cn

Table of Contents

	Page No.
Experiments detail	S3
Figure S1. Zeta potentials of Au@bPEI NCs and ZIS.....	S4
Figure S2. TEM images of ZIS nanosheets.....	S4
Figure S3. TEM images of Au@bPEI NCs.....	S5
Figure S4. UV-vis spectra of Au@bPEI NCs.....	S5
Figure S5. Blank experiments for reduction of 4-NA.....	S6
Figure S6. Photocatalytic activities of ZIS and x% Au@bPEI/ZIS.....	S6
Figure S7. UV-vis spectra of Au NPs and characterization of 3% Au NPs/ZIS.....	S7
Figure S8. Photoactivities of 3%bPEI/ZIS.....	S8
Figure S9. UV-vis spectra of bPEI and (b) XRD pattern of 3%bPEI/ZIS.....	S8
Figure S10. Photoactivities of 3%Au@bPEI/ZIS without NH ₄ COOH and adding K ₂ S ₂ O ₈	S9
Figure S11. Photoactivities of bPEI and Au@bPEI.....	S9
Figure S12. Cyclic reaction of 3%Au@bPEI/ZIS toward photoreduction of 4-NA.....	S10
Figure S13. Characterization of 3%Au@bPEI/ZIS after 5 cyclic reactions.....	S10
Figure S14. XPS spectra of 3%Au@bPEI/ZIS after cyclic photocatalytic reactions.....	S11
Figure S15. Characterization of CIS and 3% Au@bPEI/CIS.....	S12
Figure S16. Characterization of In ₂ S ₃ and 3% Au@bPEI/In ₂ S ₃	S13
Figure S17. Characterization of CdS and 3% Au@bPEI/CdS.....	S14
Table S1. Peak position with corresponding functional groups.....	S15
Table S2. Specific surface area, pore volume and pore size of ZIS and 3%Au@bPEI/ZIS.....	S15
Table S3. Chemical bond species vs. B.E. for different samples.....	S15
Table S4. Time-resolved PL decay parameters of ZIS and 3%Au@bPEI/ZIS.....	S16
Table S5. Fitted EIS results of different samples based on the equivalent circuit.....	S16
Table S6. Zeta potentials (ξ) of different samples.....	S16
Reference	S17

Experimental details

1. Preparation of CdS nanosheets^{S1}

CdS nanosheets were prepared via a hydrothermal method reported previously. In detail, 0.32 mmol CdCl₂·2.5H₂O, 2.0 mmol S powder and 12 mL of diethylenetriamine (DETA) were mixed and vigorously stirred to form a homogeneous suspension. Then, the mixture was transfer into a Teflon-lined stainless-steel autoclave with a capacity of 50 mL for 48 h at 80 °C. After cooling to room temperature, a yellowish precipitate was rinsed with deionized water and ethanol separately and dried in an oven at 60 °C for 24 h to obtain the CdS nanosheets.

2. Preparation of Ag@bPEI NCs

10 mL of AgNO₃ (10 mg/mL) and 10 mL of bPEI (25 kDa, 10 mg/mL) were added into 250 mL of DMF (10 mg/mL) and the mixture was stirred in an oil bath at 150 °C for 20 min. Subsequently, the mixture was cooled to room temperature and color of the mixture changes from transparent to brown yellow, indicative of formation of Ag@bPEI NCs (0.24 mg/mL).

3. Preparation of Pd@bPEI NCs

10 mL of Na₂PdCl₄ (20 mg/mL) and 10 mL of bPEI (25 kDa, 10 mg/mL) were added into 250 mL of DMF (10 mg/mL) and the mixture was stirred in an oil bath at 150 °C for 20 min. After reaction, color of the mixture changes from pale brown to dark gray, indicative of formation of Pd@bPEI NCs (0.26 mg/mL).

4. Preparation of Au NPs

Au NPs were synthesized by the NaBH₄ reduction of HAuCl₄.^{S2} Typically, 10 mL of 8 mM NaBH₄ was added into 10 mL of 3 mM HAuCl₄ aqueous solution. The mixture was then vigorously stirred for 10 min at room temperature until no bubbles formed in the solution. Then, the as-prepared Au NPs aqueous solution was diluted to 0.22 mg mL⁻¹.

5. Preparation of photoelectrodes

Working electrodes were prepared on fluorine-dope tin oxide (FTO) glass that was cleaned by sonication in ethanol for 30 min and dried at 353 K. The boundary of FTO glass was protected using scotch tape. The 5 mg sample was dispersed in 0.5 mL of ethyl alcohol absolute by sonication to get slurry which uniformly was spread onto the pretreated FTO glass. After drying in the air, the Scotch tape was unstuck, and the uncoated part of the electrode was isolated with nail polish. The exposed area of the working electrode was 1 cm².^{S3}

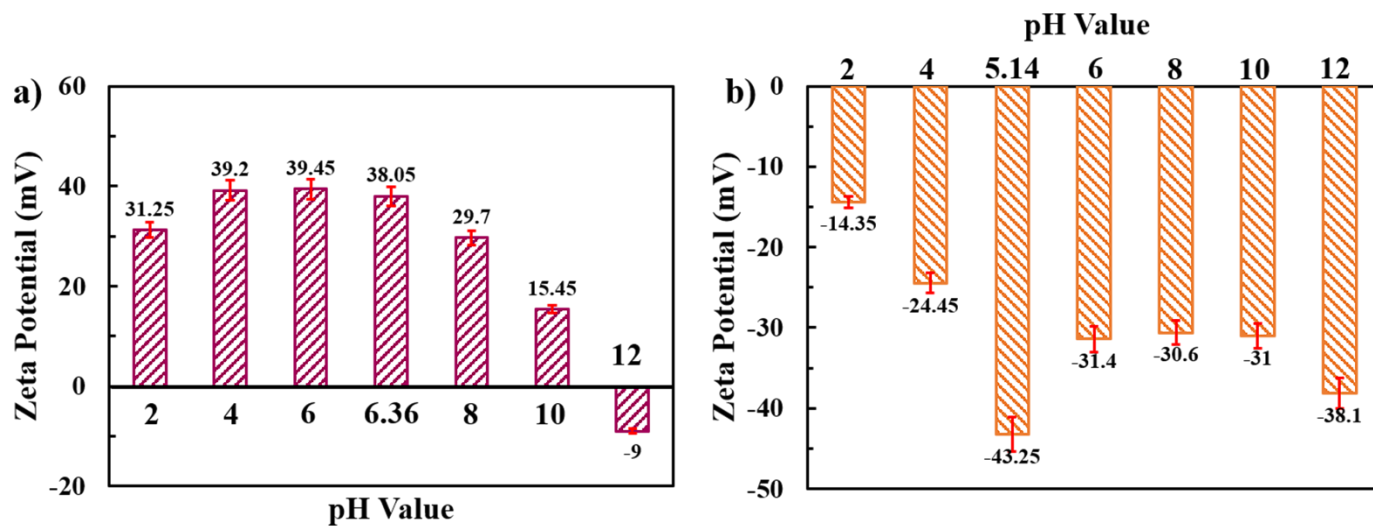


Figure S1. Zeta potentials (ξ) of (a) Au@bPEI and (b) ZIS aqueous solutions.

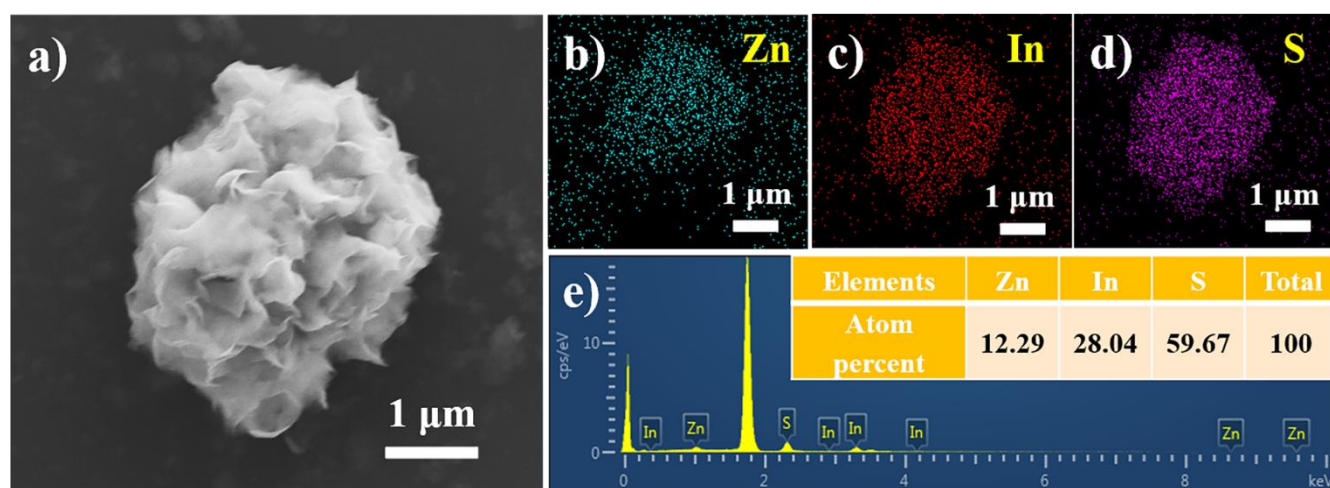


Figure S2. (a) FESEM image of ZIS nanosheets with (b-d) corresponding elemental mapping and (e) EDS results.

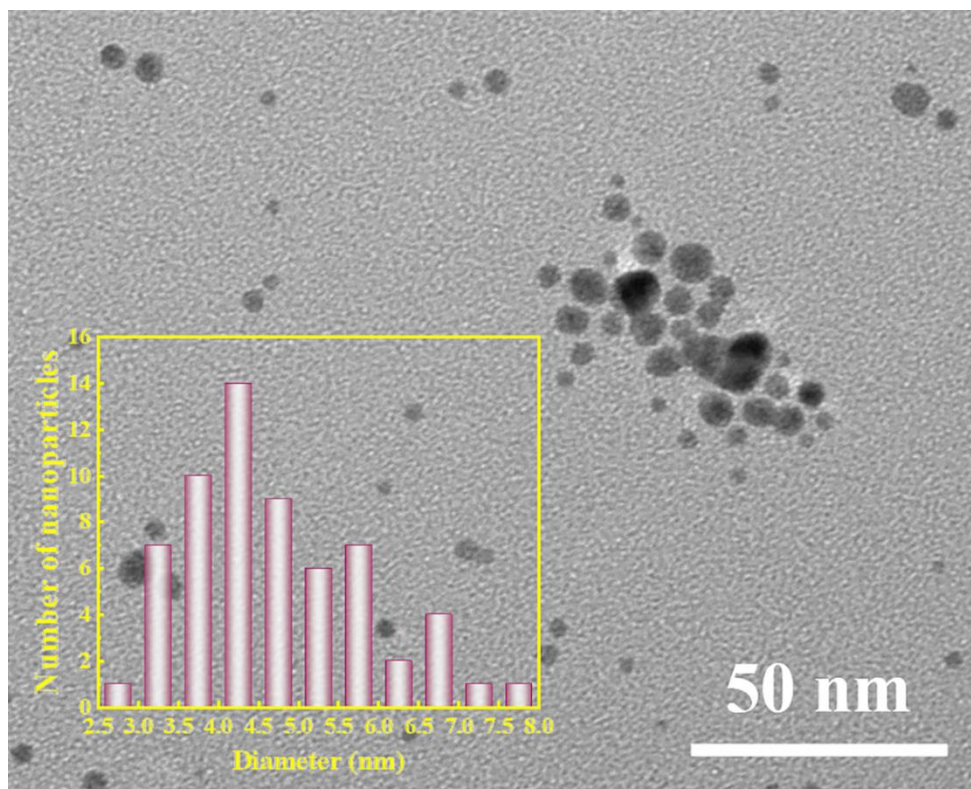


Figure S3. TEM image of Au@bPEI NCs with corresponding size distribution histogram.

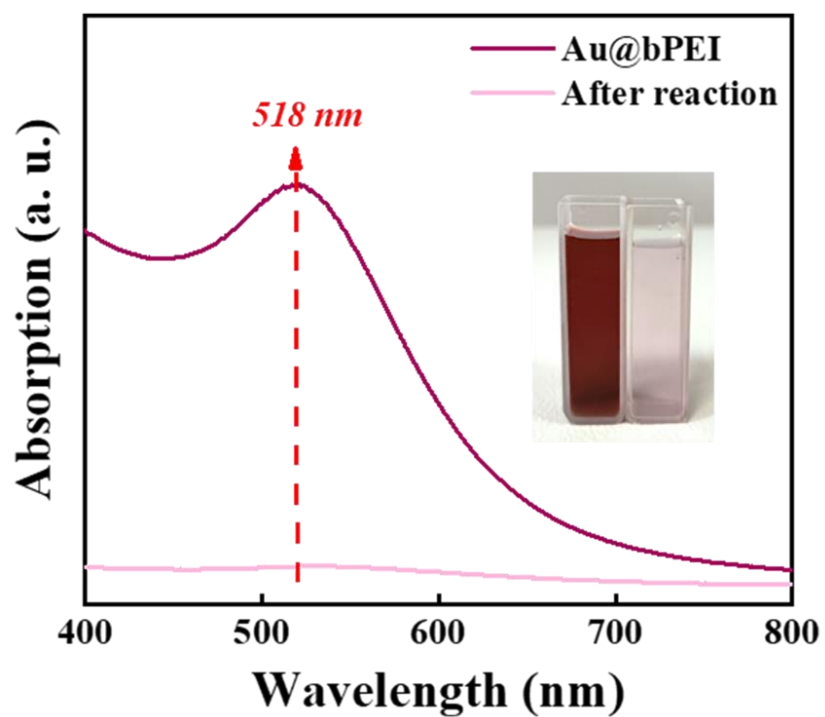


Figure S4. UV-vis spectra of Au@bPEI and supernatant after mixing with ZIS aqueous solution.

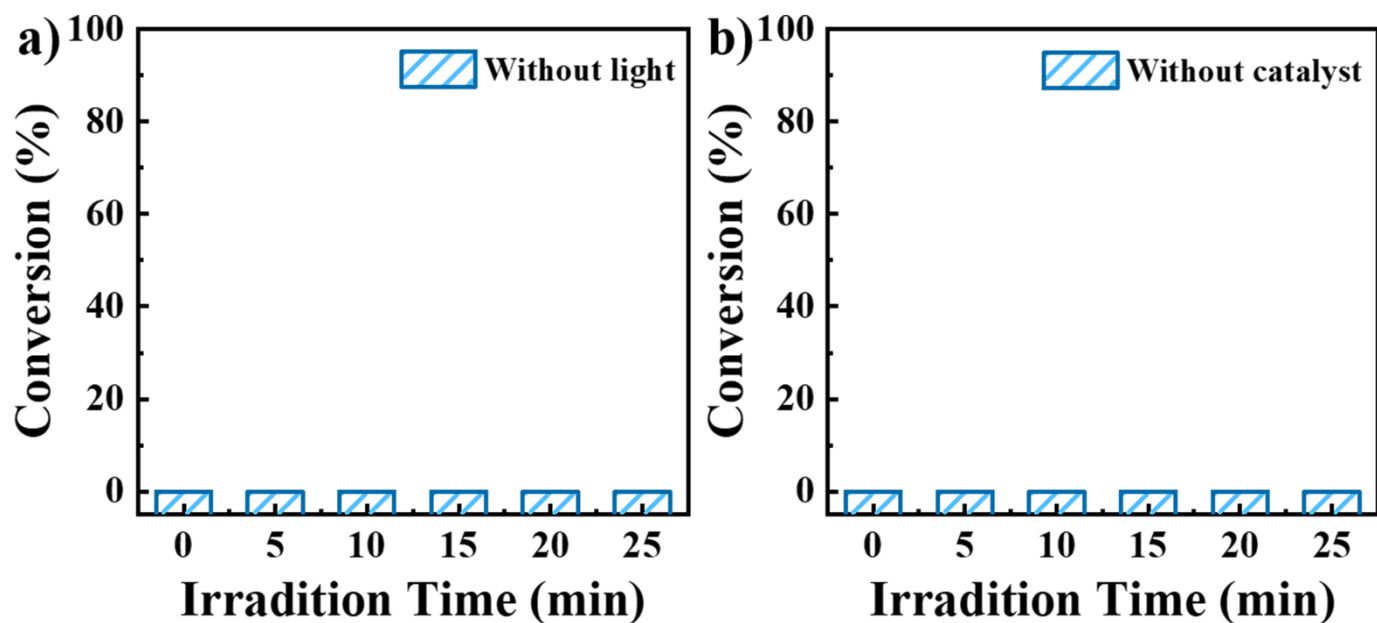


Figure S5. Blank experiments for photocatalytic reduction of 4-NA (a) without light irradiation and (b) without adding catalyst.

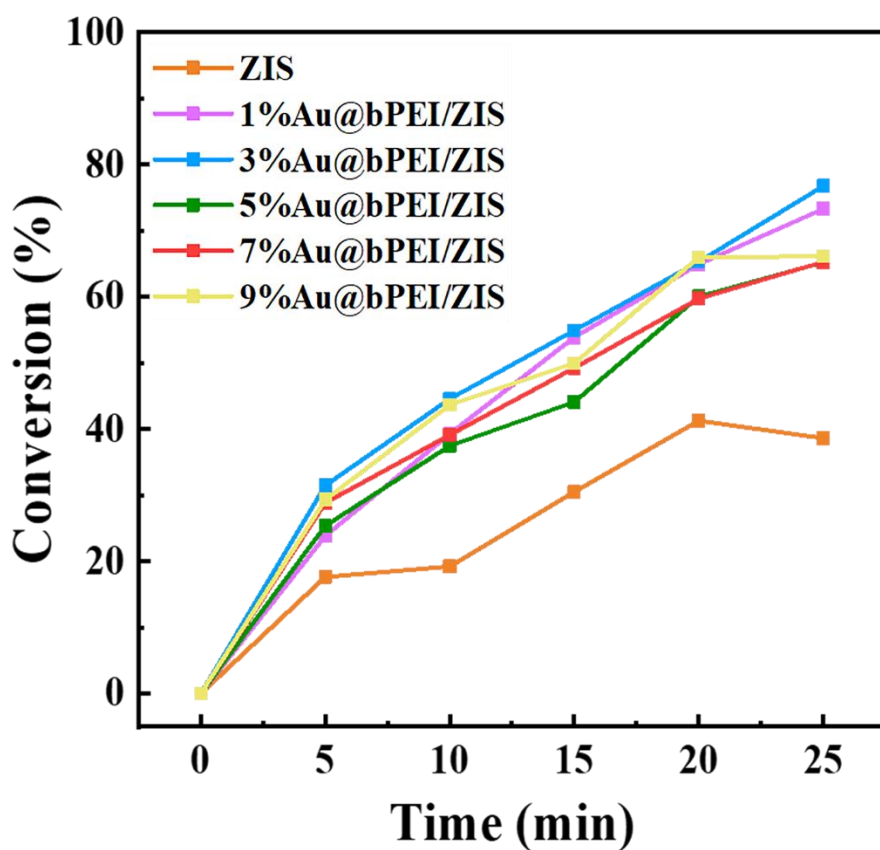


Figure S6. Photoactivities of ZIS and x%Au@bPEI/ZIS heterostructures with varying loading percentage of Au@bPEI (1, 3, 5, 7 and 9%) toward reduction of 4-NA under visible light irradiation ($\lambda > 420$ nm).

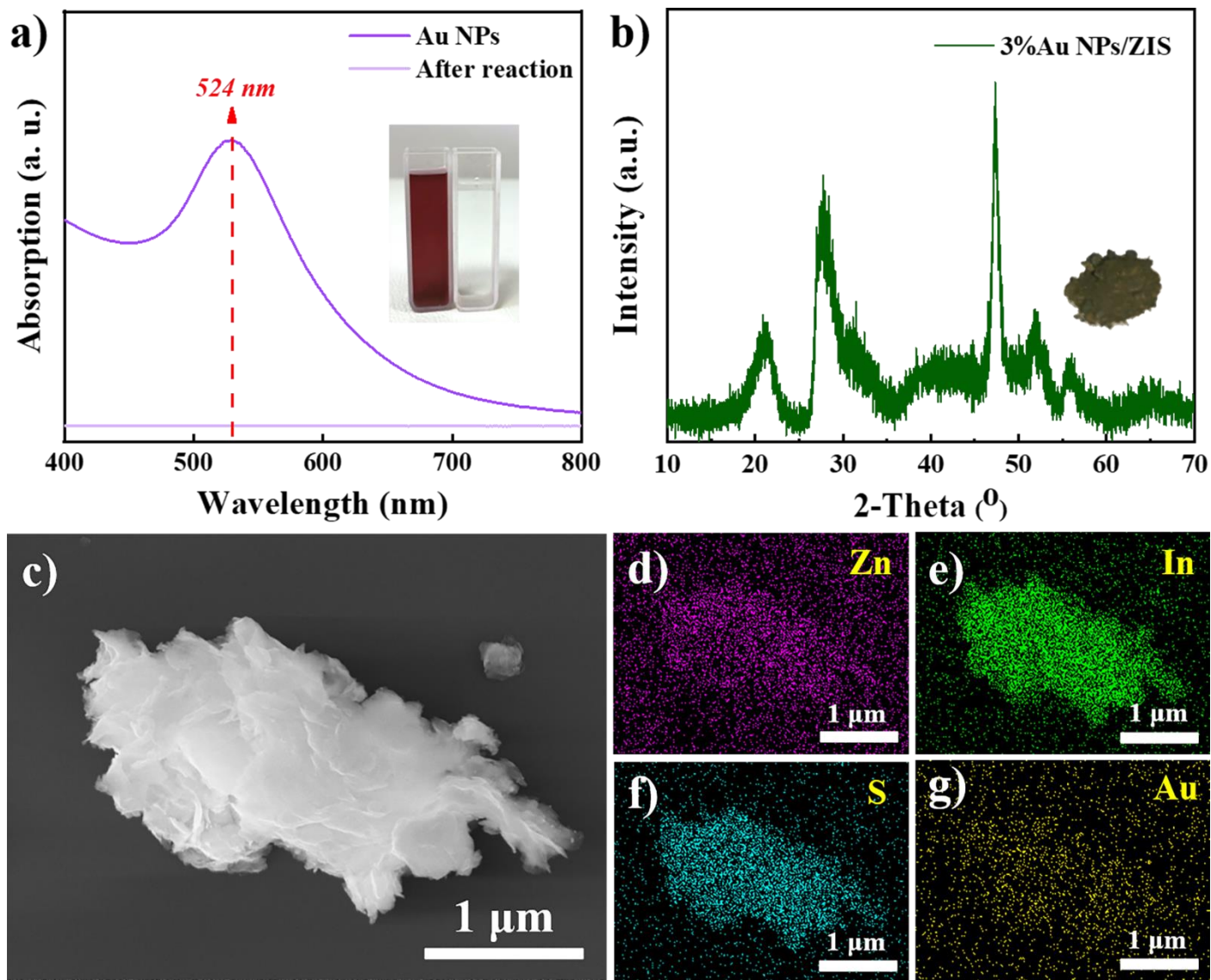


Figure S7. (a) UV-vis absorption spectrum of Au NPs and supernatant after mixing with ZnIn_2S_4 ; (b) XRD pattern of 3%Au NPs/ZIS; (c) FESEM image of 3%Au NPs/ZIS with (d-g) corresponding elemental mapping results.

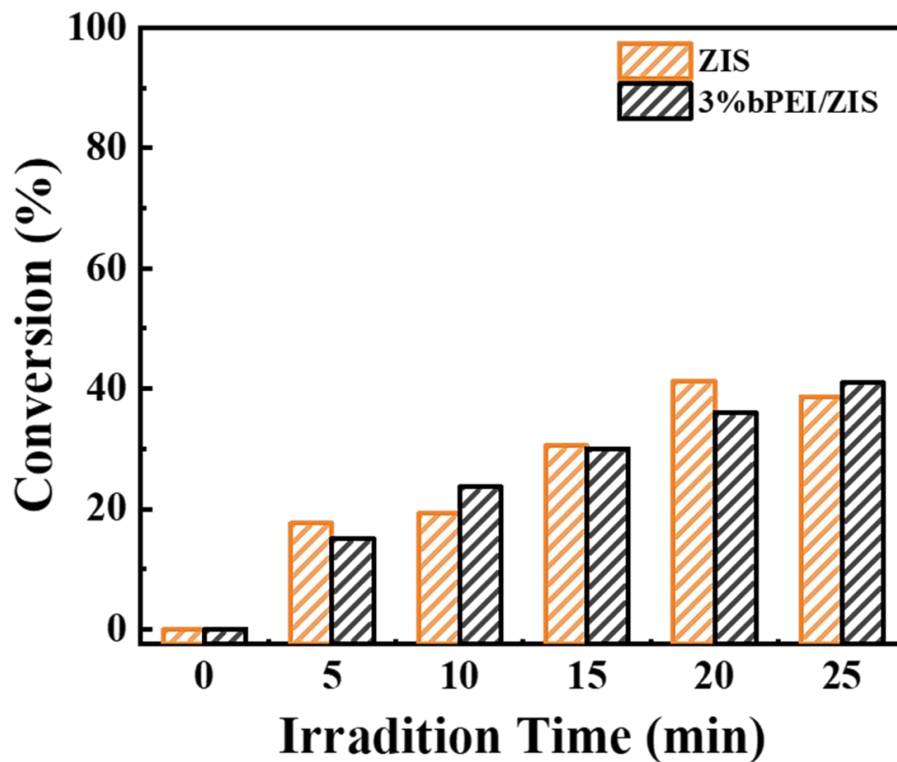


Figure S8. Photoactivity of 3%bPEI/ZIS nanocomposite toward reduction of 4-NA.

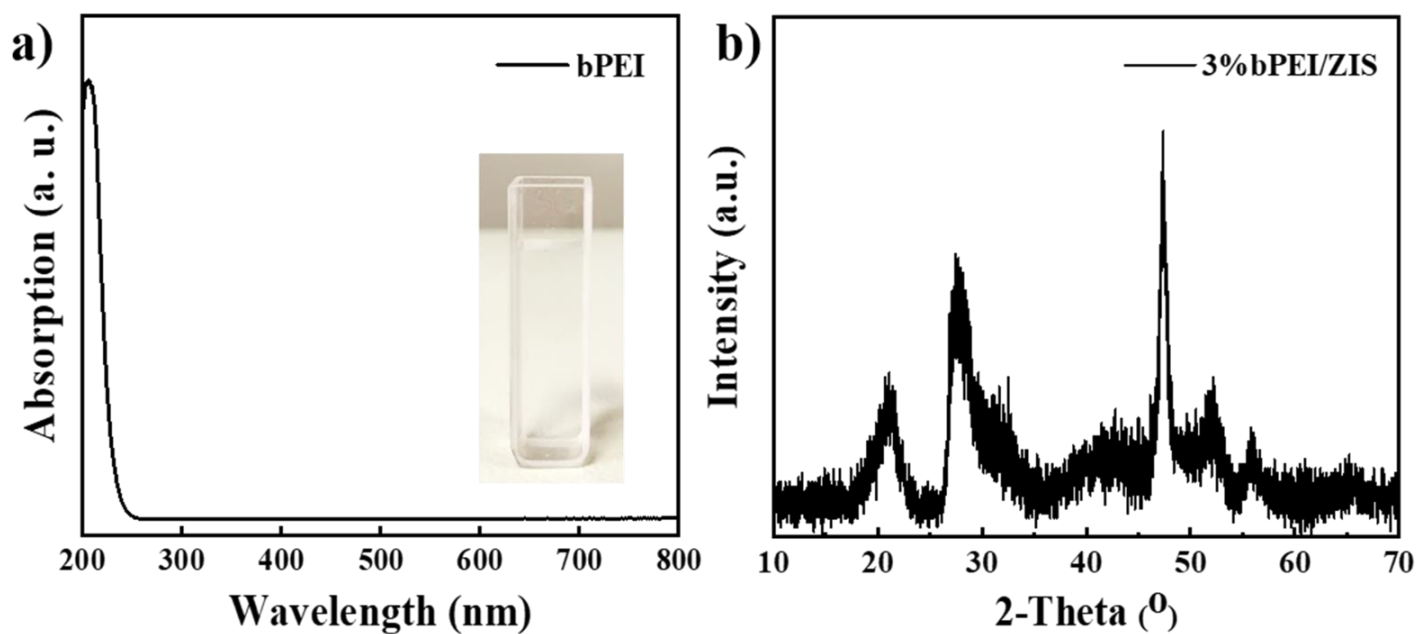


Figure S9. (a) UV-vis absorption spectrum of bPEI (10 mg/mL) and (b) XRD pattern of 3%bPEI/ZIS nanocomposite.

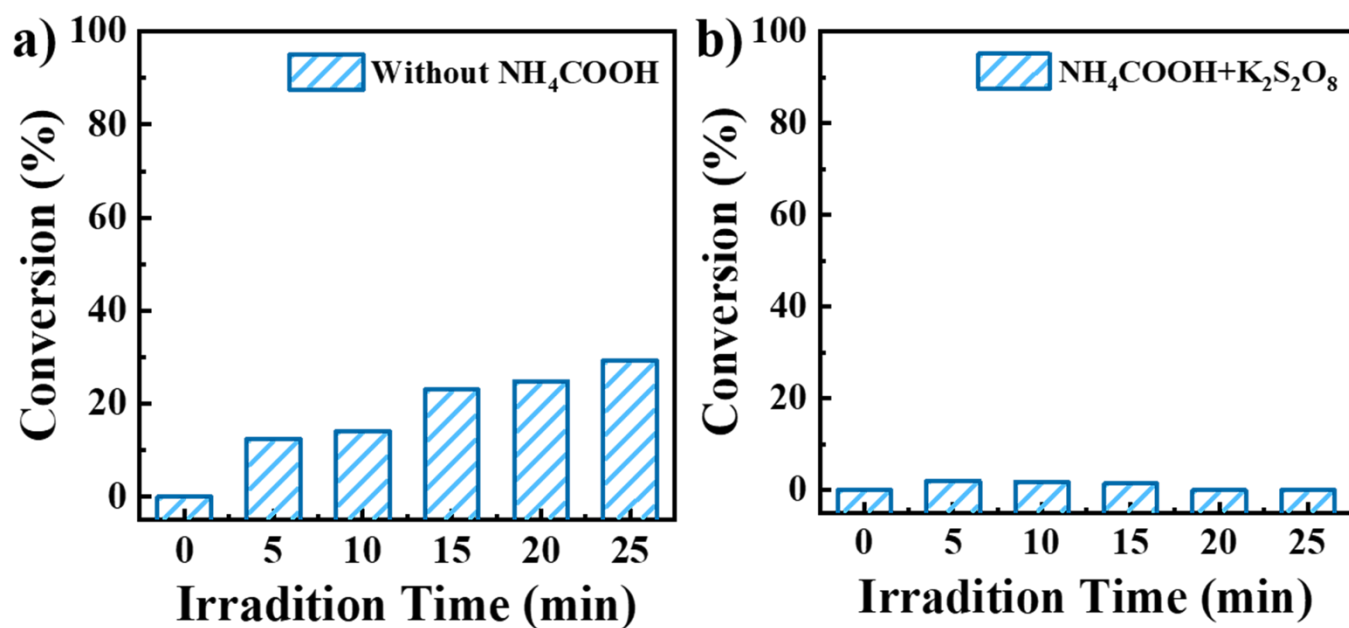


Figure S10. Photoactivities of 3%Au@bPEI/ZIS heterostructure (a) without NH₄COOH and (b) adding K₂S₂O₈.

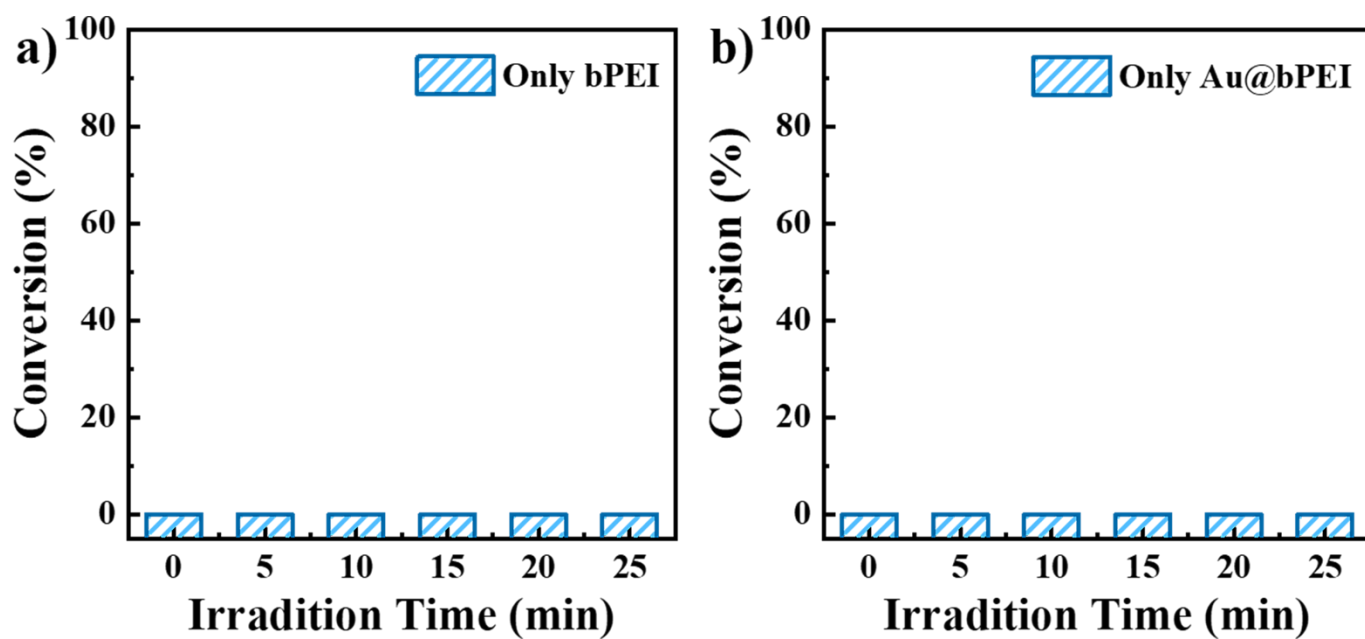


Figure S11. Photoactivities of (a) bPEI and (b) Au@bPEI toward 4-NA reduction.

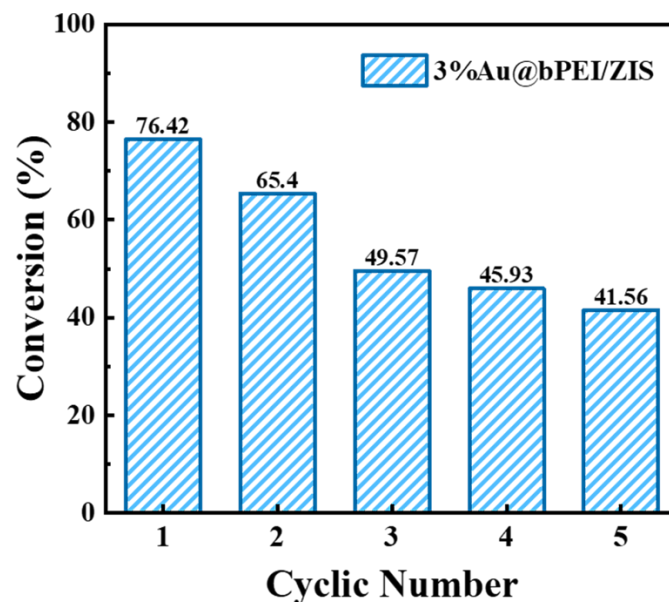


Figure S12. Cyclic reaction of 3%Au@bPEI/ZIS toward photoreduction of 4-NA under visible light irradiation.

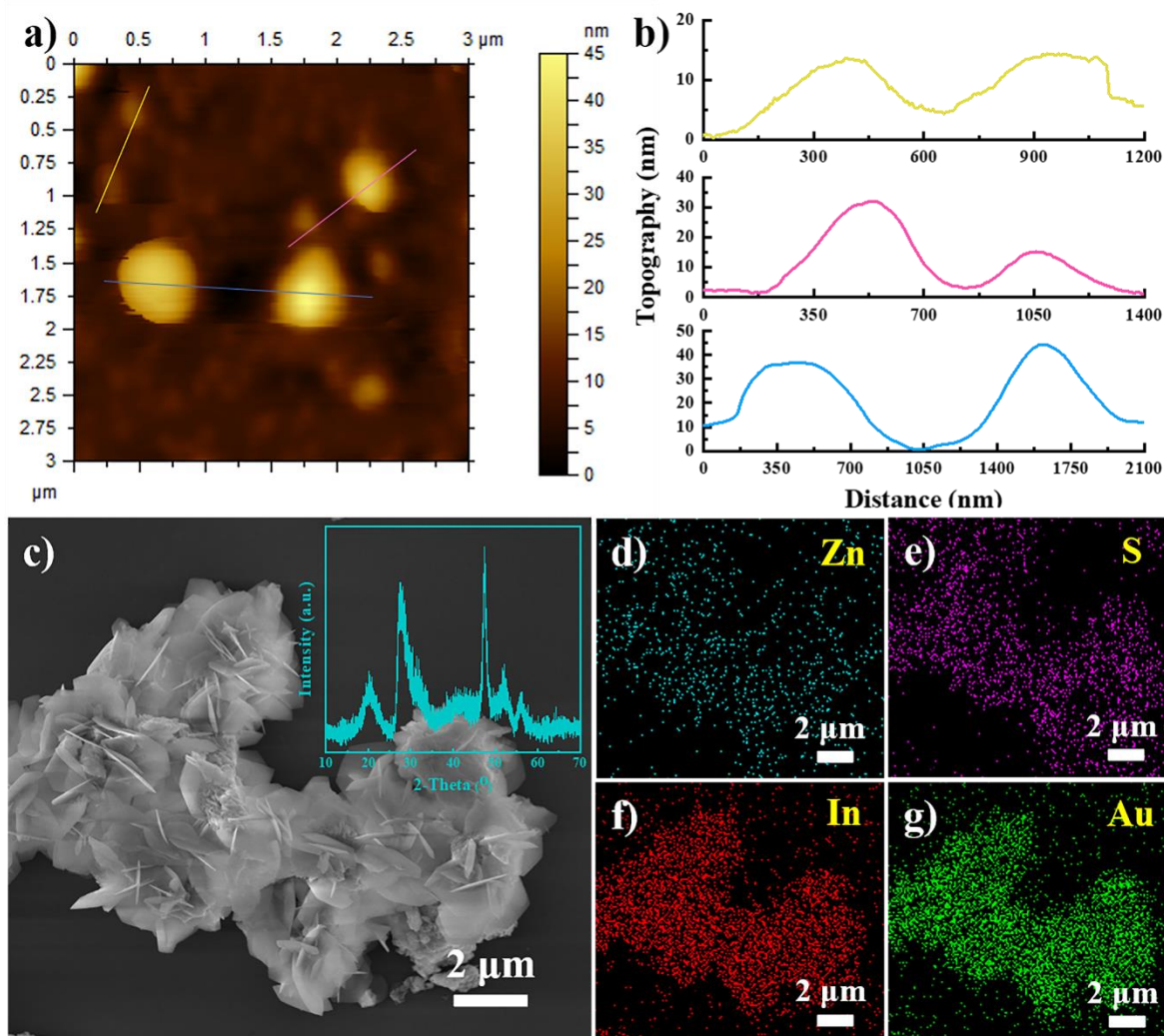


Figure S13. (a & b) AFM analysis of 3%Au@bPEI/ZIS after 5 cyclic photoreactions; (c) FESEM image of 3%Au@bPEI/ZIS heterostructure after cyclic photoreactions with (d-g) elemental mapping results. Inset shows the XRD pattern of 3%Au@bPEI/ZIS heterostructure after 5 cyclic reactions.

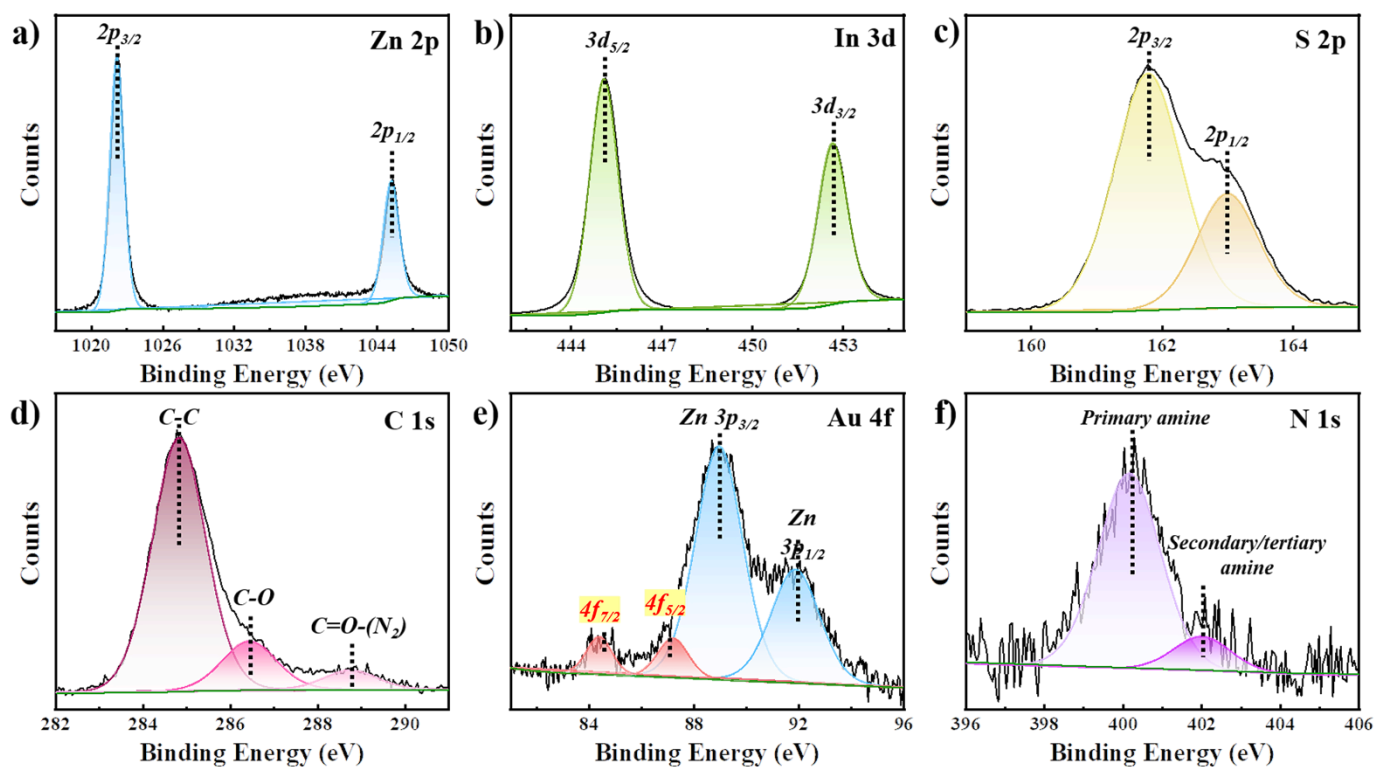


Figure S14. High-resolution (a) Zn 2p, (b) In 3d, (c) S 2p, (d) C 1s, (e) Au 4f, and (f) N 1s spectra of 3%Au@bPEI/ZIS after 5 cyclic reactions.

Note: Survey spectrum demonstrates the Zn, In and S elements, consistent with the EDS result. In the high-resolution Zn 2p spectrum, two peaks with binding energy of 1045.28 and 1022.18 eV are observed, which corresponds to the Zn(II) oxidation state of Zn element.^{S4} High-resolution In 3d spectrum shows two peaks at 445.10 eV and 452.63 eV, corresponding to the In cation with a valence of +3.^{S4} The peaks located at 161.87 and 163.23 eV are assigned to the S $2p_{1/2}$ and S $2p_{3/2}$ orbitals of divalent sulfide ions (S^{2-}),^{S5} which is in line with the elemental chemical states of $ZnIn_2S_4$. Besides, high-resolution Au4f spectrum indicates Au element is in the metallic state Au (Au^0).^{S6} The two peaks in the high-resolution N 1s spectrum centered at 400.27 and 401.93 eV are attributed to the primary and secondary/tertiary amines.^{S7} The XPS results of 3%Au@bPEI/ZIS after 5 cyclic reactions are in faithful agreement with those of pristine counterpart.

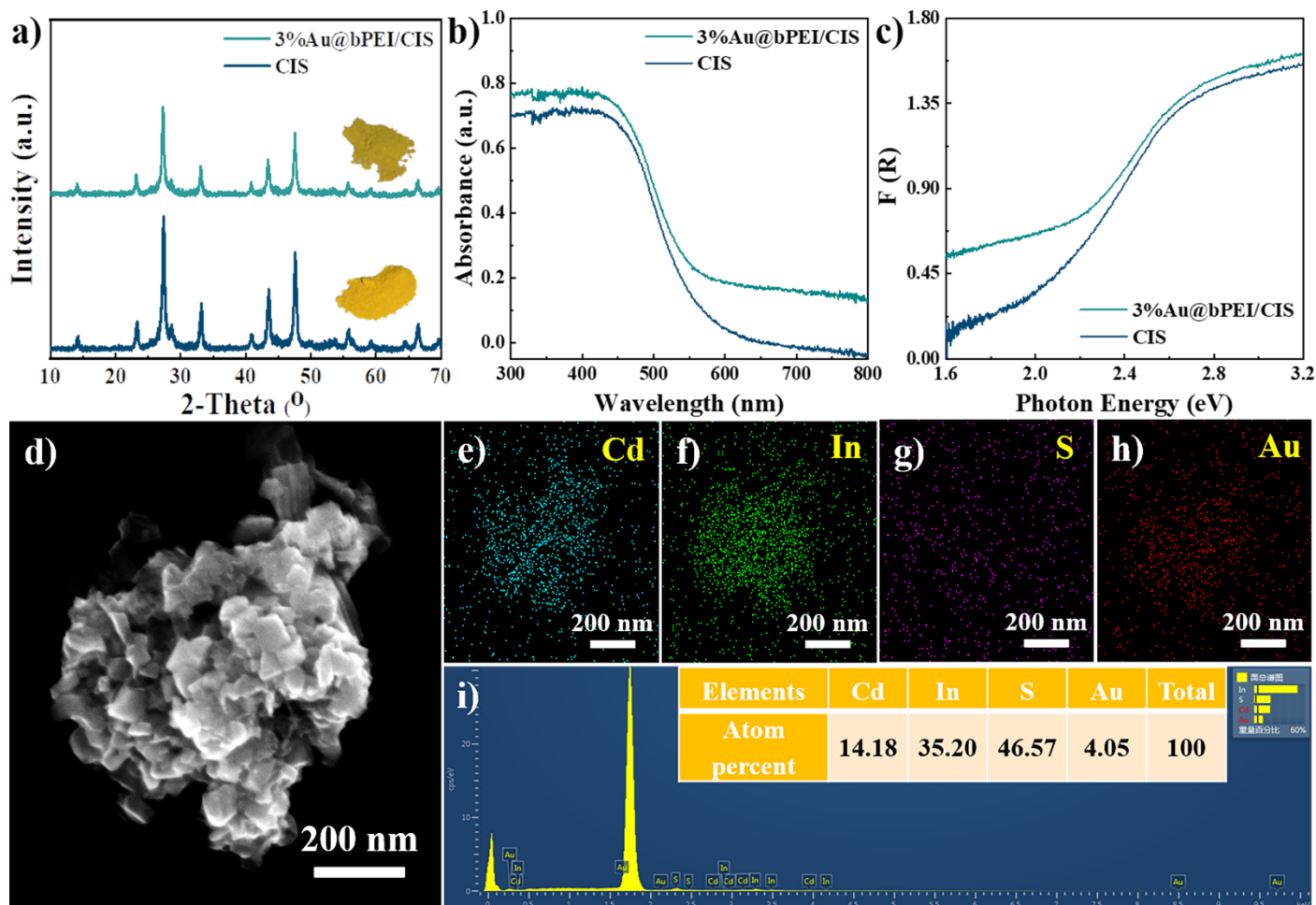


Figure S15. (a) XRD patterns of CIS and 3%Au@bPEI/CIS; (b) DRS spectra of CIS and 3%Au@bPEI/CIS with (c) transformed plots calculated based on the Kubelka–Munk function vs. the energy of light; (d) FESEM images of 3%Au@bPEI/CIS with (e-h) elemental mapping and (i) EDS result.

Note: XRD pattern of CdIn_2S_4 (**Figures S15a**) shows the high-purity cubic phase CdIn_2S_4 nanosheets (JCPDS No. 27-0060)^{S8} and 3%Au@bPEI/CIS heterostructure demonstrates the similar result. As displayed in **Figure S15(b & c)**, CIS and 3%Au@bPEI/CIS heterostructure exhibit the similar absorption edge, indicating Au@bPEI deposition does not influence the optical property of CdIn_2S_4 nanosheets. Element mapping result of 3%Au@bPEI/CIS in **Figure S15(e-h)** demonstrates the homogeneous distribution of Cd, In, S and Au signals.

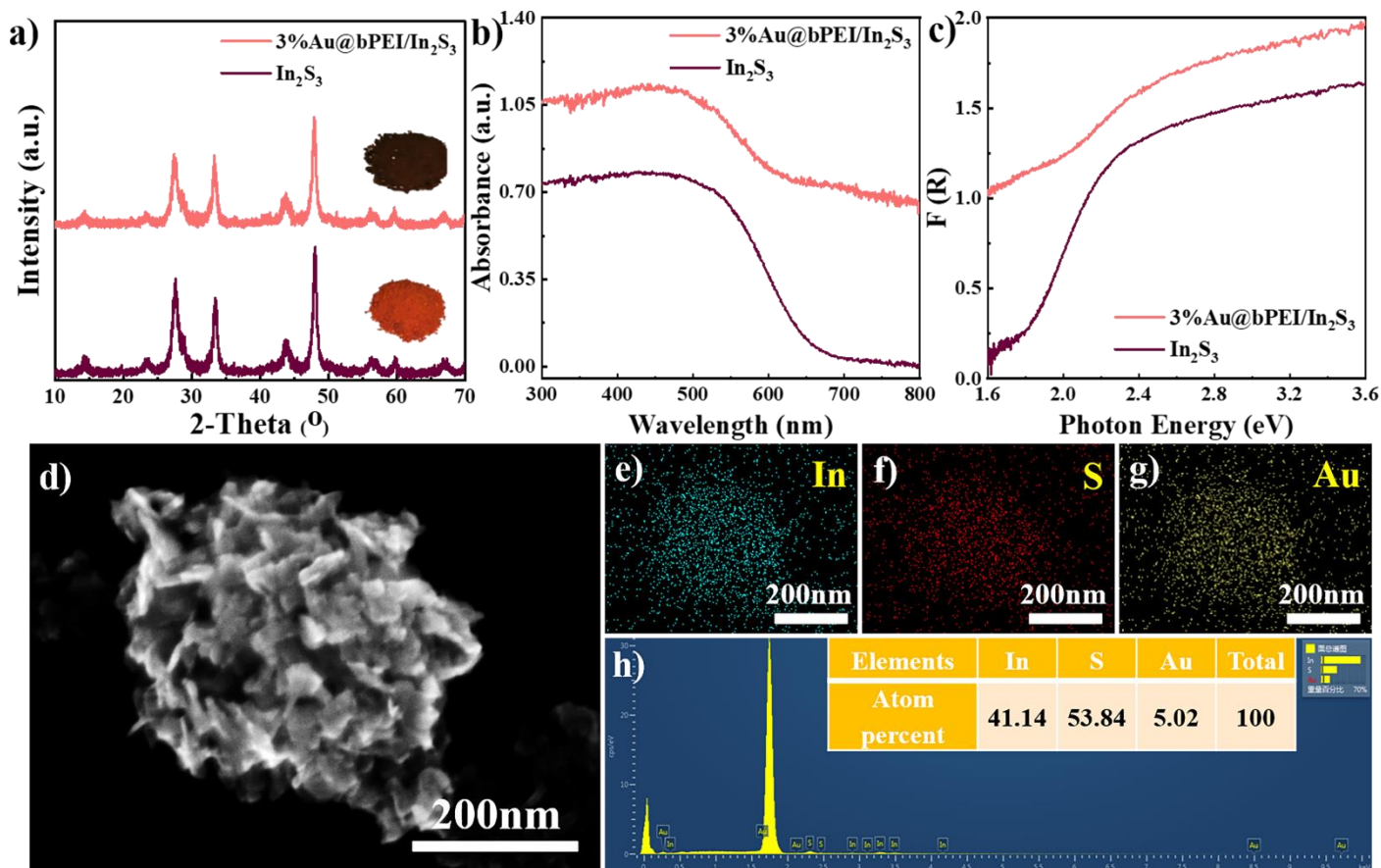


Figure S16. (a) XRD patterns of In_2S_3 and $3\% \text{Au}@b\text{PEI}/\text{In}_2\text{S}_3$; (b) DRS spectra of In_2S_3 and $3\% \text{Au}@b\text{PEI}/\text{In}_2\text{S}_3$ with (c) transformed plots calculated based on the Kubelka–Munk function vs. the energy of light; (d) FESEM image of $3\% \text{Au}@b\text{PEI}/\text{In}_2\text{S}_3$ with (e-g) elemental mapping and (h) EDS result.

Note: XRD pattern of In_2S_3 (**Figure S16a**) shows the high-purity cubic phase In_2S_3 (JCPDS No. 65-0459) and $3\% \text{Au}@b\text{PEI}/\text{In}_2\text{S}_3$ heterostructure demonstrates the similar result. As displayed in **Figure S16(b & c)**, In_2S_3 and $3\% \text{Au}@b\text{PEI}/\text{In}_2\text{S}_3$ heterostructure exhibit the similar absorption band edge position, indicating Au@bPEI deposition does not influence the optical property of In_2S_3 nanosheets. Element mapping result of $3\% \text{Au}@b\text{PEI}/\text{In}_2\text{S}_3$ in **Figure S16(e-g)** demonstrates the homogeneous distribution of In, S and Au signals.

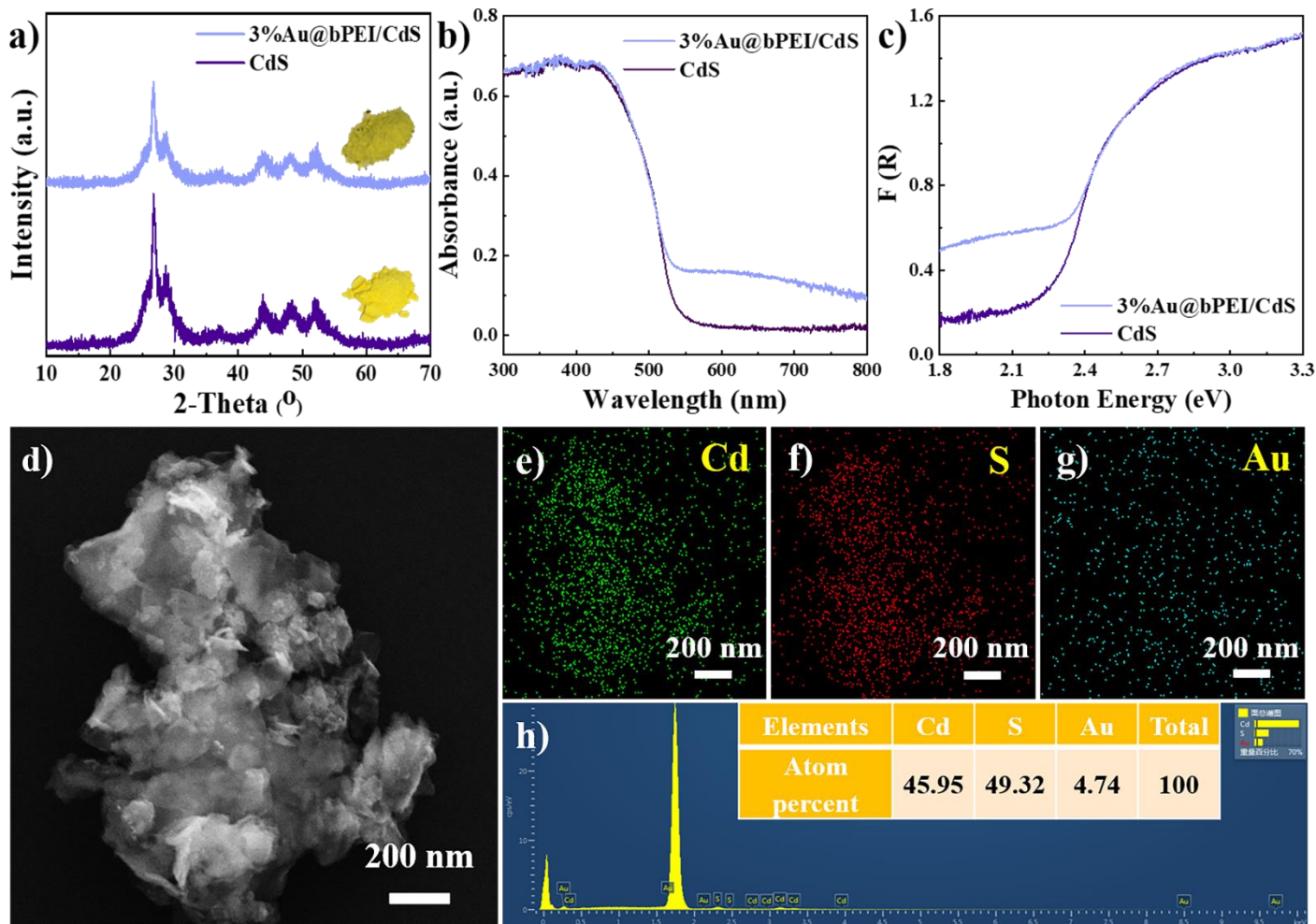


Figure S17. (a) XRD patterns of CdS and 3%Au@bPEI/CdS heterostructure; (b) DRS spectra of CdS and 3%Au@bPEI/CdS heterostructure with (c) transformed plots calculated based on the Kubelka–Munk function vs. the energy of light; (d) FESEM image of 3%Au@bPEI/CdS, (e-g) elemental mapping and (h) EDS results.

Note: XRD pattern of CdS (**Figure S17a**) shows the high-purity hexagonal phase CdS (JCPDS No. 77-2306) and 3%Au@bPEI/CdS heterostructure demonstrates the similar result. As displayed in **Figure S17(b & c)**, CdS and 3%Au@bPEI/CdS heterostructure exhibit the similar absorption intensity and absorption band edge, implying Au@bPEI deposition does not influence the optical property of CdS nanosheets. Elemental mapping results of 3%Au@bPEI/CdS heterostructure in **Figure S17(e-g)** demonstrate the homogeneous distribution of Cd, S and Au signals.

Table S1. Peak position with corresponding functional groups.

Peak position (cm ⁻¹)	Vibration mode
3430	N-H stretching vibration
1620	C=O stretching vibration
1458	CH ₂ deformation vibration
1380	CH ₃ deformation vibration
1120	C-N stretching vibration

Table S2. Specific surface area, pore volume and pore size of ZIS and 3%Au@bPEI/ZIS heterostructure.

Sample	S _{BET} (m ² /g)	Total pore volume (cm ³ /g)	Average pore size (nm)
ZIS	56.43	0.0707	2.26
3%Au@bPEI/ZIS	54.64	0.1192	3.32

Table S3. Chemical bond species vs. B.E. for different samples.

Elements	ZIS	3%Au@bPEI/ZIS	3%Au@bPEI/ZIS after 5 cycles	Chemical bond species	Ref.
Zn 2p _{3/2}	1022.18	1022.24	1022.18	Zn ²⁺	S4
Zn 2p _{1/2}	1045.18	1045.33	1045.28	Zn ²⁺	
In 3d _{5/2}	445.14	445.08	445.10	In ³⁺	S4
In 3d _{3/2}	452.68	452.63	452.63	In ³⁺	
S 2p _{3/2}	161.83	161.79	161.87	S ²⁻	S9
S 2p _{1/2}	163.13	163.08	163.23	S ²⁻	
C 1s	284.80	284.80	284.80	C-C	
C 1s	286.50	286.38	286.42	C-O	S10
C 1s	288.46	288.50	288.76	C=O-(N ₂)	
Au 4f _{7/2}	N.D.	84.37	84.40	Au ⁰	S11
Au 4f _{5/2}	N.D.	86.80	87.12	Au ⁰	
N	400.13	400.10	400.27	Primary amine	S7,
N	N.D.	401.93	401.93	Secondary/tertiary amine	S12

N.D.: Not Detected

Table S4. Time-resolved PL decay parameters of ZIS and 3%Au@bPEI/ZIS heterostructure.

Samples	τ_1 (ns)	τ_2 (ns)	A_1 (%)	A_2 (%)	τ_{ave} (ns)
ZIS	1.15	5.95	64.9	35.1	4.69
3%Au@bPEI/ZIS	0.90	5.06	70.4	29.6	3.83

Note: To quantitatively analyze the PL lifetime based on the TRPL measurement, one can use biexponential functions to fit the TRPL curves.^{S13, S14}

$$I(t) = A_1 \cdot \exp(-t/\tau_1) + A_2 \cdot \exp(-t/\tau_2) \quad (1)$$

where τ_i correspond to different positron lifetime, τ_1 is originated from the nonradiative recombination of charge carriers in the defect states of ZnIn₂S₄, τ_2 is caused by the recombination of free excitons in the ZnIn₂S₄,^{S4} A_1 , A_2 correspond to the relative intensities, while $I(t)$ is the photon counts at time t . The average lifetime (τ_{ave}) was determined by the formula below:

$$\tau_{ave} = \frac{A_1\tau_1^2 + A_2\tau_2^2}{A_1\tau_1 + A_2\tau_2} \quad (2)$$

Table S5. Fitted EIS results of different samples based on the equivalent circuit.

Sample	R_s /ohm	R_{ct} /ohm	CPE/(F·cm ⁻²)
ZIS	12.33	6253	8.538*10 ⁻⁵
3%Au@bPEI/ZIS	12.73	4713	5.507*10 ⁻⁵

Note: As shown in **Table S5**, R_{ct} values were extracted from the semicircle by fitting it according to a simple equivalent circuit (**Figure 5f, inset**)^{S15}. Apparently, 3%Au@bPEI/ZIS demonstrated smaller R_{ct} than ZIS, indicative of its lower interfacial charge transfer resistance than ZIS.

Table S6. Zeta potentials (ξ) of different samples.

Sample	pH value	Zeta potential (mV)
Ag@bPEI	7.70	55.05
Pd@bPEI	9.19	20.85
CdIn ₂ S ₄	4.73	-11.65
In ₂ S ₃	4.88	-28.80
CdS	5.33	-35.75

References

- S1. X. Xie, N. Zhang, Z.-R. Tang, M. Anpo and Y.-J. Xu, *Appl. Catal. B: Environ*, 2018, **237**, 43-49.
- S2. F. Xiao, Y. Zheng, P. Cloutier, Y. He, D. Hunting and L. Sanche, *Nanotechnology*, 2011, **22**, 465101.
- S3. T. Li, Y.-B. Li, X.-C. Dai, M.-H. Huang, Y. He, G. Xiao and F.-X. Xiao, *J. Phys. Chem. C*, 2019, **123**, 4701-4714.
- S4. M. Q. Yang, Y. J. Xu, W. Lu, K. Zeng, H. Zhu, Q. H. Xu and G. W. Ho, *Nat. Commun.*, 2017, **8**, 14224.
- S5. S. Wang, B. Y. Guan and X. W. D. Lou, *J. Am. Chem. Soc.*, 2018, **140**, 5037-5040.
- S6. F. X. Xiao, S. F. Hung, J. Miao, H. Y. Wang, H. Yang and B. Liu, *Small*, 2015, **11**, 554-567.
- S7. D. Pakulski, W. Czepa, S. Witomska, A. Aliprandi, P. Pawluć, V. Patroniak, A. Ciesielski and P. Samorì, *J. Mater. Chem. A*, 2018, **6**, 9384-9390.
- S8. Q. Zhang, J. Wang, X. Ye, Z. Hui, L. Ye, X. Wang and S. Chen, *ACS Appl. Mater. Interfaces*, 2019, **11**, 46735-46745.
- S9. S. Zhang, X. Liu, C. Liu, S. Luo, L. Wang, T. Cai, Y. Zeng, J. Yuan, W. Dong, Y. Pei and Y. Liu, *ACS Nano*, 2018, **12**, 751-758.
- S10. Y. Li, J. Cai, M. Hao and Z. Li, *Green Chem*, 2019, **21**, 2345-2351.
- S11. X.-C. Dai, M.-H. Huang, Y.-B. Li, T. Li, S. Hou, Z.-Q. Wei and F.-X. Xiao, *J. Phys. Chem. C*, 2020, **124**, 4989-4998.
- S12. Y. B. Li, T. Li, X. C. Dai, M. H. Huang, S. Hou, X. Y. Fu, Z. Q. Wei, Y. He, G. Xiao and F. X. Xiao, *ACS Appl. Mater. Interfaces*, 2020, **12**, 4373-4384.
- S13. S. Cao, J. Zhao, W. Yang, C. Li and J. Zheng, *J. Mater. Chem. C*, 2015, **3**, 8844-8851.
- S14. J. Song, C. Ma, W. Zhang, S. Yang, S. Wang, L. Lv, L. Zhu, R. Xia and X. Xu, *J. Mater. Chem. B*, 2016, **4**, 7909-7918.
- S15. Z.-Q. Wei, X.-C. Dai, S. Hou, Y.-B. Li, M.-H. Huang, T. Li, S. Xu and F.-X. Xiao, *J. Mater. Chem. A*, 2020, **8**, 177-189.